Lithospheric strength controls transform zone structure

O. Dauteuil, Olivier Bourgeois, T. Mauduit

Geophys. J. Int. (2002) **150,** 706–714

Lithosphere strength controls oceanic transform zone structure: insights from analogue models

O. Dauteuil,[1] O. Bourgeois[2] and T. Mauduit[1]

[1] *Géosciences Rennes, Université de Rennes* 1, 35042 *Rennes Cedex, France. E-mail: dauteuil@univ-rennes1.fr*
[2] *ENSG (CRPG-CNRS) rue du Doyen Marcel Roubault, BP* 40, 54 501 *Vandoeuvre-lès-Nancy Cedex*

Accepted 2002 March 15. Received 2002 March 12; in original form 2001 June 10

SUMMARY

Oceanic transform zones have often been regarded as plate boundaries. The origin of their structural variability is poorly constrained. A simple observation indicates that the transform zone is narrow and linear when the offset is large; while it is wide with a complex faulting pattern in the case of a small offset. On the other hand, for a given offset, large structural differences exist between transform zones located on the fast-spreading South-East Pacific Rise and on the slow-spreading Mid-Atlantic ridge. In general, the transform zones in slow-spreading environments are linear with a simple fault pattern, while in fast-spreading systems they are wide with a complex pattern of deformation. We perform small-scale analogue modelling to constrain the influence of lithospheric strength on the development of deformation above a transform boundary. The models are made up of sand and silicone putty as analogues of the brittle layer and the viscous layer of the lithosphere, respectively. Two plastic sheets coming from shifted gashes form a set-up of two diverging discontinuities connected by a transform boundary. The rheological layering and strength of the model were modified using different shapes of the viscous layer placed on the transform boundary. Above the divergent discontinuities, the faulting pattern is always formed by parallel normal faults. When no viscous layer is placed on the transform boundary (strong discontinuity), the deformed zone is narrow and has few linear faults. By adding a narrow and thin viscous layer, the deformed zone becomes wider with a complex faulting pattern formed by oblique-slip faults on the limits and by pure strike-slip faults in the inner part. These latter strike-slip faults trend oblique to the transform boundary. When a viscous layer with a wide lateral extent overlays the transform discontinuity (weak strength), the faulting is dominated by obliquely normal faults extending over a wide zone, and the strike-slip is restricted to the inner part of the deformed zone. Therefore, the mechanical strength of the small scale-model controls the shape of the deformed zone and the deformation partitioning. These results were applied to 24 oceanic transforms zones: we point out that the spreading rate and the transform offset are the two dominant parameters controlling the deformation pattern. These two factors directly control the lithospheric strength at the transform boundary. However, the distance to the nearest hotspot, which may generate warmer thermal conditions even in slow-spreading environments, should modify this result.

Key words: analogue modelling, lithospheric strength, transform zones.

1 INTRODUCTION

Transform zones (TZs) are major structures offsetting oceanic ridges. They display different structural patterns depending on the geodynamic context. In slow-spreading contexts, such as the Mid-Atlantic Ridge (MAR), the TZs appear as deep narrow linear valleys, filled by sediment and trend at high angles to the rift axis (Fig. 1a). In fast-spreading contexts, such as the southern part of the East Pacific Rise (EPR), the transform zones are wider and contain complex arrays of strike-slip faults often separated by small spreading segments (Fig. 1b). In North Iceland, the Tjörnes Fracture Zone is located above a hotspot in a slow-spreading context. This TZ is very wide (Fig. 1c) and composed of strike-slip faults, which are associated with horsts and grabens, parallel to the ridge axis (MacMaster *et al.* 1977; Bourgeois 1998).

On the whole, TZs differ according to: (1) width (narrow on the MAR and the northern EPR, wide on the southern EPR and ultrawide near the the hotspot); (2) fault orientation (the range of fault orientation increases from slow- to fast-spreading contexts); (3) deformation partitioning between strike-slip and normal faults;

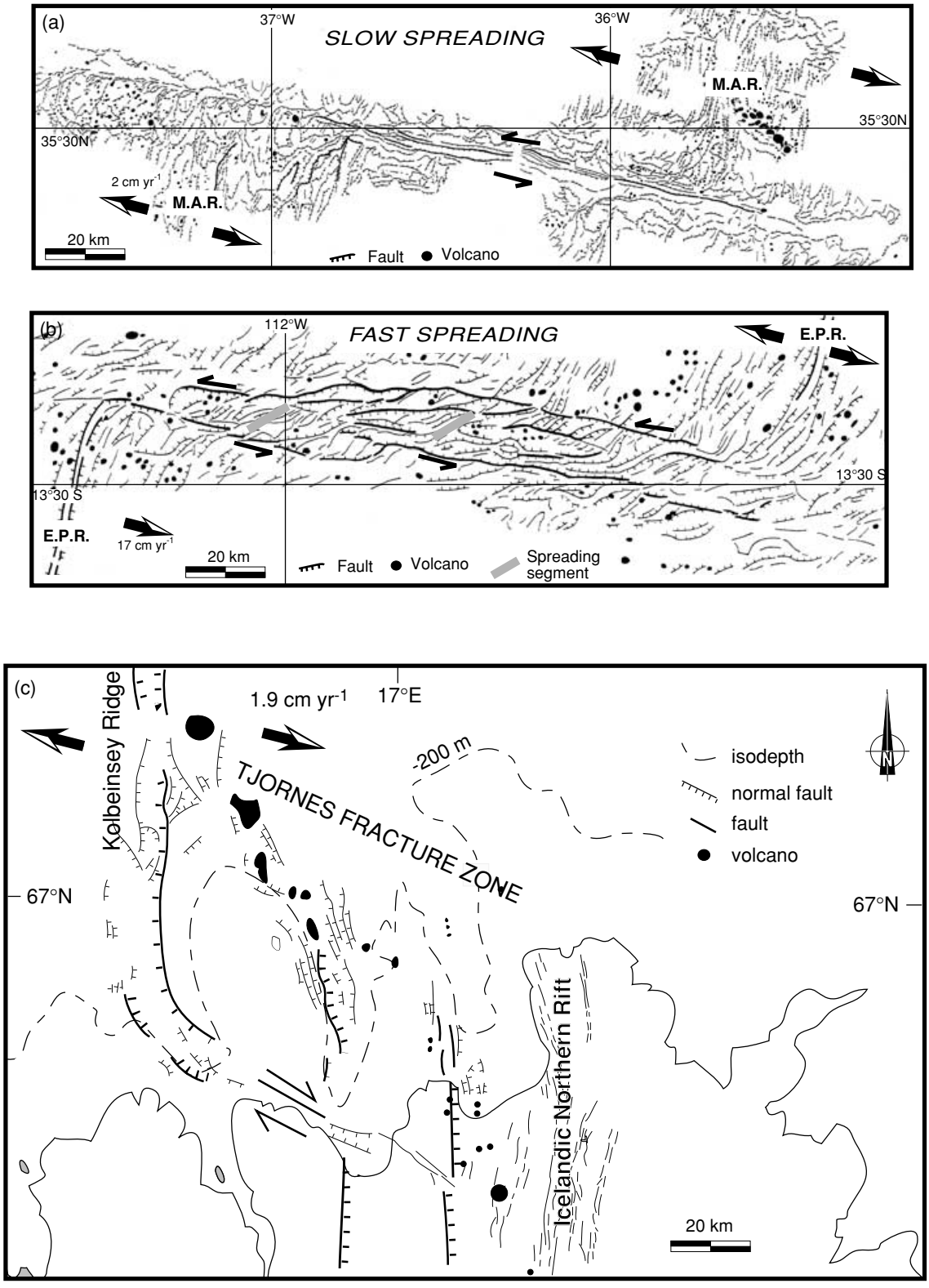

Figure 1. Fault patterns in oceanic transform zones. (a) Oceanographer Transform Zone on the Mid-Atlantic Ridge, (b) Garrett Transform Zone on the East-Pacific Rise, and (c) Tjörnes Transform Zone in Iceland. Lengths of lateral offsets are equivalent (110–130 km). Variation in spreading rates or special regional contexts contribute to such structural differences, in addition to transform zone length as demonstrated by Mauduit & Dauteuil (1996).

and (4) depth with a decrease of the mean depth of the deformed zone from MAR to Iceland.

Few studies have explored the reasons for such differences. On the basis of analogue modelling, Mauduit & Dauteuil (1996) and Acocella *et al.* (1999) pointed out the relationship between the length of transform offset and the width of the deformed zone; namely, the longer the offset, the narrower the transform zone. This effect, however, cannot explain structural differences between

transform zones with similar offsets such as the Garret TZ (southern EPR), the Oceanographer TZ (MAR) and the Tjörnes TZ (Iceland) (Figs 1a and c). More generally, the results of Mauduit & Dauteuil (1996) are in good agreement with data from the MAR but do not fit with data from the EPR, where TZs are systematically wider than predicted. Alternatively, the spreading rate affects the structure of oceanic ridges considerably (Macdonald 1982; Choukroune *et al.* 1984) and might explain structural differences between TZs with similar offsets. This was suggested but not demonstrated first by Stoddard (1992) and more recently by Tuckwell *et al.* (1999). This explanation, however, does not hold for TZs with different structures, only those with similar spreading rates such as, for instance, the Tjörnes and Oceanographer TZs, both located on the MAR.

A significant input controlling the deformation pattern of a structure is the lithospheric strength (e.g. Buck 1991; Grindlay & Fox 1993; Kohlstedt *et al.* 1995; Benes & Davy 1996). Bergman & Solomon (1992) conclude from an earthquake analysis that the lithosphere on TZ is weaker than the surrounding lithosphere. This mechanical strength is controlled by the thermal state, the strain rate and the composition of the lithosphere. In an oceanic domain, the strain rate can be assumed to be constant and the lithospheric composition can be simplified to two rheological end-members: the crust and the mantle. However, the thermal structure is correlated both to the spreading rate and the distance to the nearest hotspot. Near a TZ, the thermal state also depends on the transform length, on the spreading rate and on the regional heat flow. For a given spreading rate and regional heat flow, higher spreading rates yield higher thermal gradients because of the shallow depth of the isotherms (Chen 1989; Lin & Parmentier 1989, 1990; Mauduit & Dauteuil 1996). In addition, the presence of a hotspot below the TZ can increase the regional heat flow. The thermal gradient controls the thickness of the upper brittle layer of the lithosphere given by the depth the 750 °C isotherm (Lin & Parmentier 1990; Chen & Phipps Morgan 1996) and the viscosity of the underlying ductile layer. The brittle layer thickness and the viscosity of the ductile layer directly control the bulk strength of the lithosphere (Davy *et al.* 1995): increases of thickness and/or of the viscosity make the lithosphere stronger.

Therefore, we investigated the influence of the bulk lithospheric strength and of the rheological layering on the deformation patterns at TZs, through mechanical experiments performed on small-scale models. The experiments explore the effect of two parameters on the deformation induced by a transform boundary: the strength of the lithosphere with depth and the width of the weak zone above the transform boundary. Previous, analogue models (Mauduit & Dauteuil 1996; Acocella *et al.* 1999) analysed the effect of the shape of the transform discontinuity, but not the influence of the rheological layering and of the lithospheric strength. Our study is focused on TZs, away from the ridge axis where the rheological structure is complex and variable because of the presence of magma chambers (Shaw & Lin 1996; Lagabrielle *et al.* 2001).

2 ANALOGUE MODELLING

Our approach is based on deformation simulations in small-scale models having different rheological layering. Natural materials can be considered as having two main rheological behaviours (brittle or viscous), depending on temperature, strain rate, composition and deformation condition (extension, strike-slip or compression). These four parameters control the rheological layering of the lithosphere, i.e. a succession of brittle and ductile layers, and the whole strength of the lithosphere. The estimate of the strength profile versus depth gives a good image of the rheological layering through the different change in profile shape, and can evaluate the whole strength that is given by the surface integration of the profile (Kohlstedt *et al.* 1995).

In our models, the rheological structure of the lithosphere is simplified as a system composed of a brittle layer overlaying a ductile layer (Watts *et al.* 1980; Dauteuil & Brun 1993; Thibaud *et al.* 1999). The brittle part of the lithosphere is modelled with a 3-cm thick layer of sand, a Mohr–Coulomb material a density ranging from 1.5 to 1.7 g cm^{-3}, depending on the way the layers were laid. The ductile part is modelled by viscous putty, a Newtonian fluid with a viscosity of 4×10^4 Pa s and a density of 1.2 g cm^{-3} (Weijermars 1986a,b; Davy & Cobbold 1991; Dauteuil & Brun 1993; Thibaud *et al.* 1999).

The experimental apparatus is similar to that used by Mauduit & Dauteuil (1996). It is composed of two diverging plate boundaries representing oceanic ridges, offset by a transfer discontinuity representing a transform zone (Fig. 2a). The two junctions between the transfer discontinuity and the diverging boundaries are referred to as 'the intersections' hereafter. The angle between the diverging plate boundaries and the spreading direction is 90°. The transfer discontinuity is parallel to the spreading direction. The whole thickness of the model is fixed by the lithospheric strength that inhibits surface deformation when it is too strong (Dauteuil & Brun 1993; Mauduit & Dauteuil 1996). This threshold approximately fits to a depth out of axis of the oceanic rift. So we simplify the natural system outside the ridge axis by a single layer of sand, analogue to a brittle layer. Beneath the axis of oceanic ridges, a wedge of hot ductile material exists close to the surface (Lin & Parmentier 1989). The wedge has roughly a triangular shape in cross-section because isotherms deepen away from the spreading axis. In our experiments, a triangular wedge of viscous putty that was put on the diverging boundary models this isotherm pattern (Fig. 2b). This wedge is 1.5 cm in height and has a width that varyies depending on the experiment. The models are set up on a table. Divergence is achieved by two plastic sheets located at the base of the model, emerging from two gashes offset by up to 25 cm (see Mauduit & Dauteuil 1996, for a complete description of the apparatus). The viscous layer overlays the plastic sheets and is covered by sand. By pulling the two sheets, extension is imposed at the base on the viscous layer that deforms itself. All experiments were performed with the same divergence rate (4 cm h^{-1}) and were stopped after a total displacement of 2 cm. A grid of white sand, initially drawn on the surface of the model was used to quantify the deformation. The scaling ratios between the experiment and nature are: 10^{-5} in height, 4×10^{-5} in length and 8.77×10^{-9} in time (1 h corresponds to 1 Myr).

To investigate the effects of rheological layering and lithospheric strength on the deformation patterns in TZs, a viscous layer made up of silicone putty is placed along the transfer discontinuity in some experiments. This viscous layer locally decreases the strength of the whole system. Different configurations were tested (Fig. 3). In the first experiment (FT 1), designed to model a strong TZ ('cold' lithosphere), no silicone putty was placed along the transfer discontinuity (Fig. 3a). In the second experiment (FT 2), designed to model a weak TZ ('hot' lithosphere), a narrow silicone band was placed above the transform boundary (Fig. 3b). In the last experiment (FT 3), designed to model a wide weak zone ('hot' lithosphere), a wide silicone layer was placed above both the spreading and transform discontinuities (Fig. 3c).

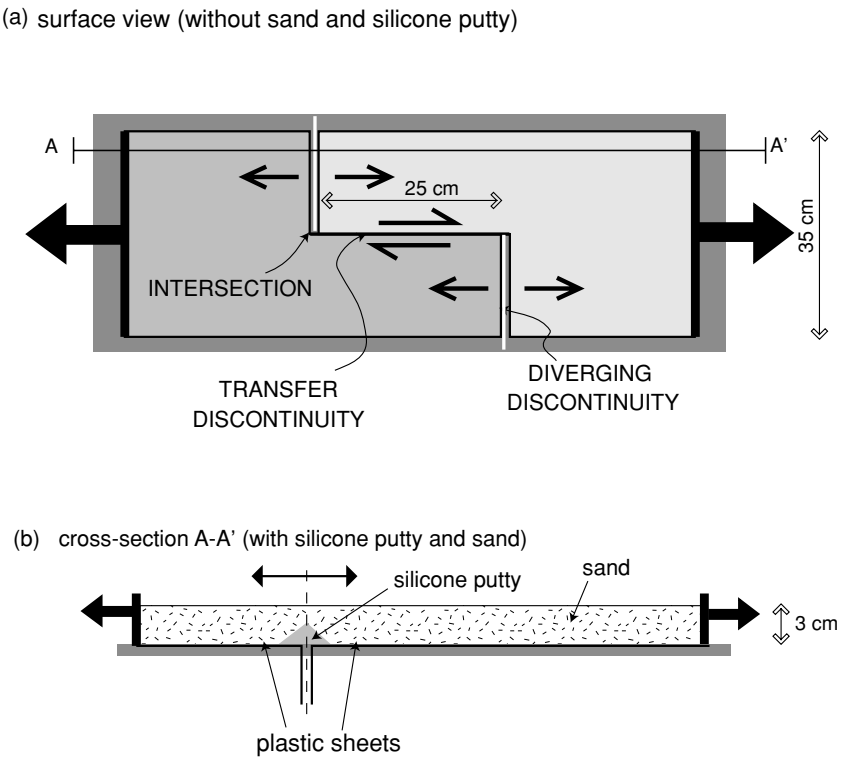

Figure 2. Experimental apparatus (Mauduit & Dauteuil 1996). Two plastic sheets fixing the deformable thickness of the model diverge from two gashes, 25 cm apart. The gashes from where the plastic sheets go out, define the diverging discontinuities. A triangular layer of silicone putty is placed on this diverging discontinuity as analogue of the hot part of the lithosphere of the oceanic rift. The plastic sheets are pulled at 4 cm hr^{-1} by a stepping motor. The divergent motion of the sheets induced a deformation to the model. The surface view (a) shows the different boundaries of the apparatus and the cross-section (b) a section of the experiment above the diverging boundary (see the location in a).

3 EXPERIMENTAL RESULTS

3.1 Diverging discontinuities

Deformation patterns on the diverging boundaries are very similar for all the experiments (Fig. 4). First, a pair of symmetric normal faults with inward dips is generated close to each divergent axis. These faults are parallel to the diverging boundaries. After 33 per cent extension, new inward faults appear between the previous faults that become inactive as they drift away from the boundaries. At the end, four faults (two inactive and two active) had formed for each diverging boundary, forming a set of stair step blocks.

3.2 Strong transform zone: experiment FT 1

In this model (Figs 3a and 4a), the deformed zone above the strike-slip discontinuity is 1.2 cm deep, 0.8 cm wide at the centre of the TZ and up to 2 cm wide at the intersections, at the end of the experiment. It is formed by two oblique-slip faults trending nearly as the discontinuity. Connection between these oblique-slip faults and normal faults of the diverging discontinuity is achieved by a horsetail set of secondary faults, dipping toward the diverging discontinuity. This horsetail pattern is associated with widening of the deformed zone. Angles between faults and the transfer discontinuity increase from 10° at the centre to 25° at the intersections. At the intersections, outer corners are formed by step-by-step curved faults displaying both strike-slip and normal throws. In contrast, inner corners are composed of single active curved faults. Strike-slip motions are distributed between two faults in the central part of the TZ and distributed between all the horsetail faults at the intersections.

3.3 Weak transform zone: experiment FT 2

In this model (Figs 3b and 4b), the zone above the strike-slip discontinuity affected by the deformation is 0.8 cm deep, 3 cm wide at the centre of the TZ and up to 4 cm wide at the intersections. There are two sets of faults in the central part of the TZ. The first set, which appear early in the deformation, trend at 30° to the discontinuity direction and show horizontal and vertical displacements. The second set forms later during deformation at the margins of the deformed zone, and trends at 15° to the discontinuity direction. It mainly accommodates strike-slip displacement. Therefore, the strike-slip component increases outwards in the deformed zone. The dip-slip component of the first set increases toward the intersections. Connection between strike-slip faults of the TZ and normal faults of the diverging boundaries is achieved by a horsetail fault array. The horsetail faults, located at the outer corner, have a curved shape bounding asymmetric lenses. They accommodate the largest vertical motions of the deformed zone.

3.4 Wide weak zone: experiment FT 3

In this model (Figs 3c and 4c), the deformation associated with the strike-slip discontinuity affect a zone 0.7 cm deep, 7 cm wide at both the centre and the ends of the TZ. It trends at 35° to the

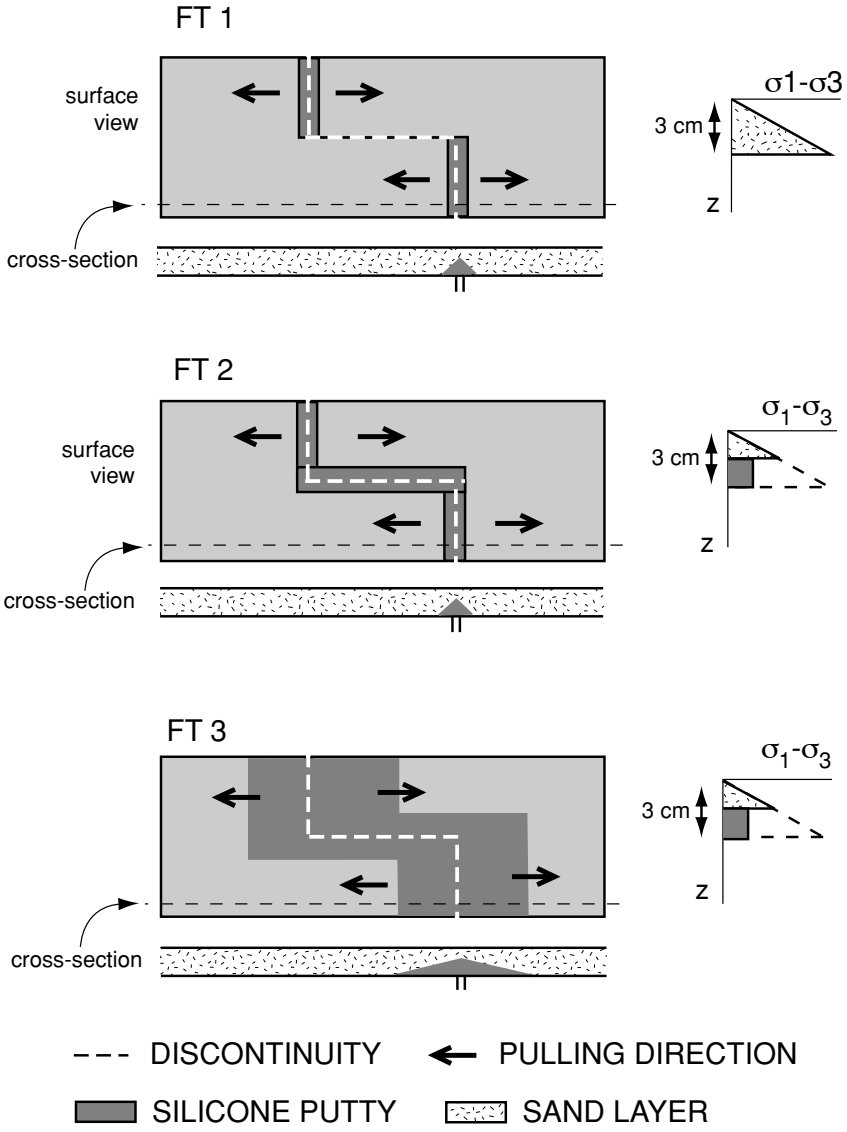

Figure 3. Experimental settings: FT 1 without a silicone band on the transform discontinuity; FT 2 with a narrow silicone band on the transform discontinuity; FT 3 with a wide silicone band. For each setting a surface view and a cross-section located above the diverging discontinuity are displayed. Strength profiles at the centre of the strike-slip boundary are illustrated on the right.

discontinuity. It overlaps the deformed zone associated with the diverging boundaries. Two fault sets affect the deformed area above the strike-slip discontinuity. The first set trends at 30°–35° to the discontinuity direction and forms early. It is made up of long normal faults with vertical throws decreasing toward their tips. The horizontal displacement along them is small. The second set is composed of purely strike-slip faults parallel to the discontinuity and are localized in the central part of the deformed zone. This later fault set appears a few times after the first set. Above this discontinuity, the oblique normal faults swing into parallel with the strike-slip faults. The two fault sets bound asymmetric lenses disposed *en échelon*. The faults of the first set largely go beyond the transfer boundary and affect the inner corner of the intersection. They reach the normal faults of the diverging discontinuities. These faults have an oblique-slip component: the strike-slip component tends to decrease far away from the transfer discontinuity. The outer corners of the intersection display *en-échelon* patterns of numerous curved faults.

4 DISCUSSION

4.1 Interpretation of the results

This experimental modelling clearly shows how the mechanical strength and the rheological layering control the deformation pattern. When no viscous layer is present on the transfer discontinuity (experiment FT 1), lateral shearing imposed by the boundary conditions mainly generates two strike-slip faults slightly oblique to the discontinuity. These faults correspond to R-faults in Riedel's model of failure of brittle rocks (Riedel 1929). R′ faults predicted by Riedel's model, however, do not appear in our models, probably because the amount of deformation is too small.

By adding a viscous layer on the discontinuity (experiments FT 2 and FT 3), two sets of fault are generated: the first one trends at 30° to the transfer discontinuity and the second one, appearing later, at 15° (R faults of Riedel's model). Riedel's model does not

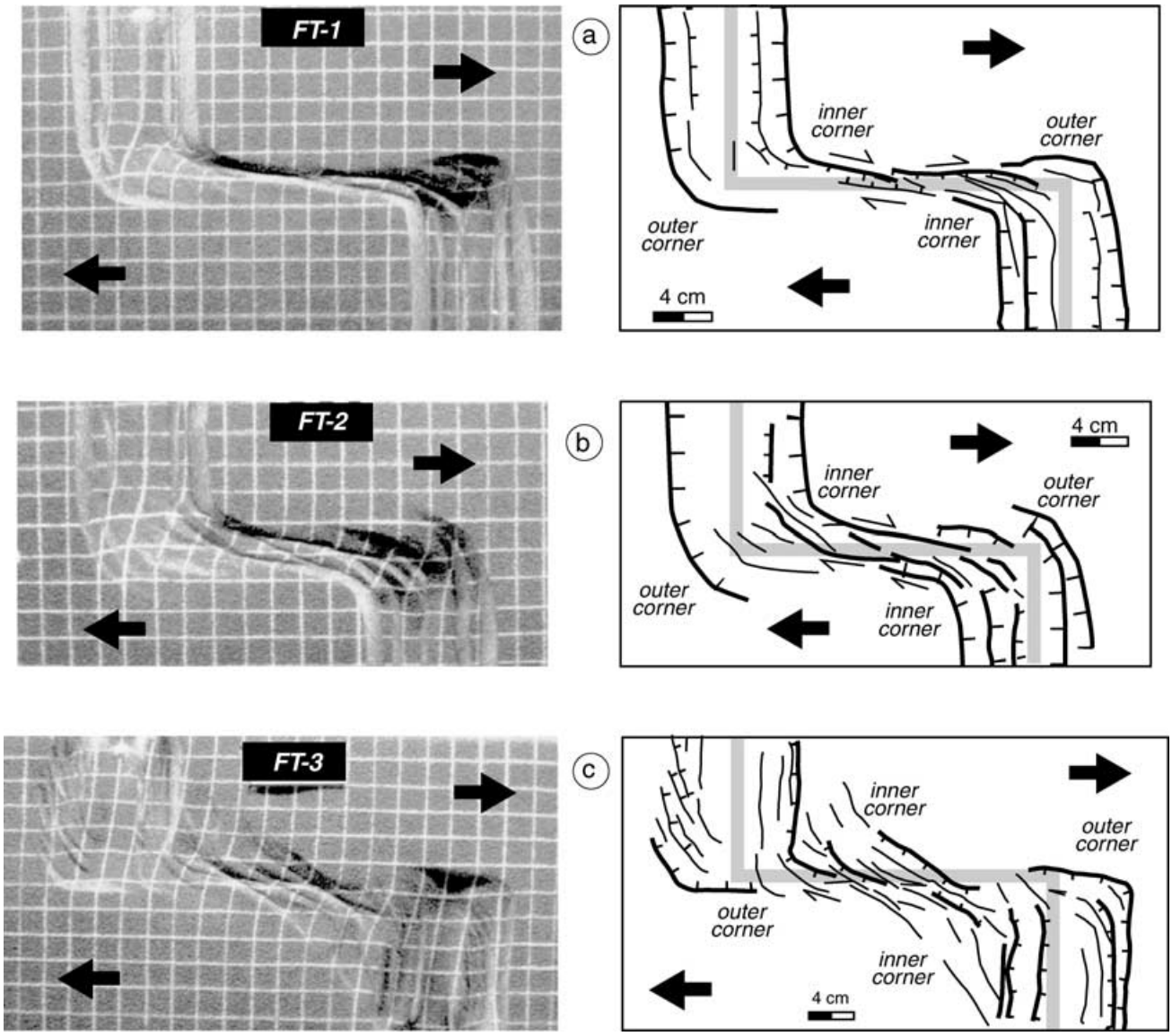

Figure 4. Experimental results. The left-hand column displays surface views of the experiments at the end of the deformation. The right-hand column shows sketch drawings of fault patterns. The light grey line indicates initial location of diverging and transfer discontinuities. Black arrows indicate the movement direction. From top to bottom, the deformed zone widens, the number of normal faults and the number of strike-slip fault oblique to the transform trend increases. The lines of the white grid are spaced at 2 cm.

predict faults trending at 30° to the strike-slip direction. Dauteuil & Mart (1998) however, described such faults in small-scale experiments on two-layer models. Therefore, this oblique fault set appears to be symptomatic of strike-slip deformation of the brittle–ductile systems.

The deformation is partitioned between oblique-slip faults bounding the deformed zone and a rather pure strike-slip fault inside the deformed zone; these latter faults often trend close to the discontinuity direction (Fig. 4). The vertical displacement along the faults becomes the main motion component when the fault direction and the transfer discontinuity has an angle greater than 25°. This is observed along the curved faults located at the intersections: their vertical throws increase as they become parallel to the diverging discontinuity. We suggest that oblique faults are in a configuration, relative to the spreading direction, in favour of dip-slip motions.

The width of the deformed zone ranges from 0.8 cm in models without a ductile layer (experiment FT 1) to more than 5 cm in models with a wide viscous layer (experiment FT 3). Widening of the deformed zone is associated with an increase of the number of active faults and a decrease of the distance between faults. A similar widening of deformed zones and an increase of fault quantities in the presence of a ductile layer have been described previously in purely extensive and in oblique rifting contexts (Tron & Brun 1991; Dauteuil & Brun 1993; Benes & Davy 1996; Thibaud *et al.* 1999). In our experiments, widening of the deformed zone is also associated with an increase in obliquity between the deformed zone and the transfer discontinuity (Fig. 5).

Changes in width and obliquity of the deformed zone are associated with changes in the partitioning of strike-slip and dip-slip motions along faults. There are more oblique faults, and consequently more normal faults, when the deformed zone is wide (experiments FT 2 and FT 3) than when it is narrow (experiment FT 1). Differences in the width of TZ are associated with differences in deformation partitioning: by increasing the width, extensional structures are

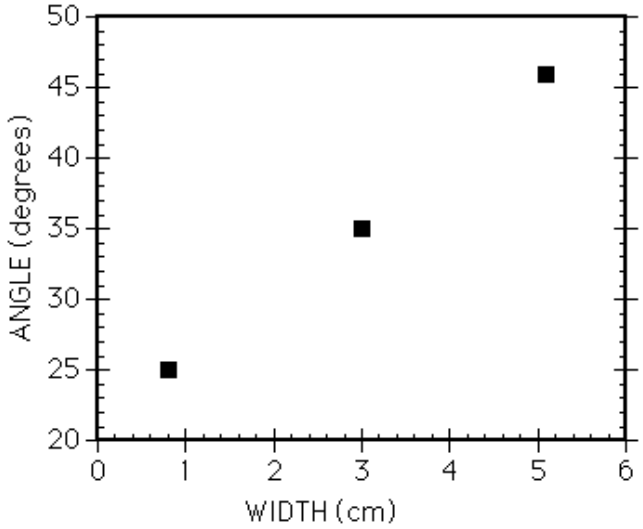

Figure 5. Angles between faults and transfer discontinuity plotted against width of the deformed zone. Measurements were made at the end of the experiments. The width is measured at the middle section of the deformed band.

generated more easily. When the deformed zone is narrow, extension and strike-slip motions are focused on the boundary faults. When the deformed zone is wide, a partitioning between normal and strike-slip motions occurs: strike-slip displacements are located along faults slightly oblique to the pulling direction, while normal faults are largely oblique. The location of these two fault sets and the relative length depend on the width of the viscous, i.e. of the width weak zone. If it is narrow, the normal faults are short and confined by the strike-slip faults, while if it is wide the normal faults are long and cross the whole deformed zone, and the strike-slip faults are confined to the central part of the strike-slip boundary.

In summary, the presence of a viscous layer along the transfer discontinuity decreases the lithospheric strength in the TZ and diffuses the deformation imposed by the plastic sheets by a flowing of this viscous layer. It results in a width increase and an orientation change of the deformed zone. It also affects partitioning of strike-slip and dip-slip motions along faults. On the whole, it allows genesis of complex deformation patterns with faults largely oblique to the transfer discontinuity. Width, obliquity and partitioning are also controlled by the offset length: an increase of the offset diminishes the width and the obliquity of the deformed zone and limits the deformation partitioning (Mauduit & Dauteuil 1996; Acocella *et al.* 1999). Similar partitioning was estimated from numerical modelling (Phipps Morgan & Parmentier 1984; Grindlay & Fox 1993). Therefore, a widening of the viscous layer above the strike-slip discontinuity and a decrease of the offset has the same effect on deformation patterns. We suggest that this convergence can be explained by the interference of the two diverging discontinuities: interference is substantial both when these two discontinuities are close to each other or when deformation can be diffused into a wide zone via a viscous layer.

4.2 Implications for natural examples

Mauduit & Dauteuil (1996) pointed out the relationship between the length of lateral offset and the width of transform zones. The experiments presented here show that TZ structures are also controlled by the lithospheric strength and the flowing of the deep layer. In natural cases, the lithospheric strength at TZ depends on a combination of several parameters including the spreading rate, regional heat flow, composition and TZ offset. The first three physical parameters are common for any natural system. However, in the case of the oceanic transform zones, the transform length is another important geometrical input: for a given spreading rate, the smaller the TZ, the lower the thermal contrast is between two adjacent plates and the hotter the lithosphere (Phipps Morgan & Forsyth 1988).

Plots of widths and spreading rates coming from 24 transform zones show that the TZ width increases with the spreading rate (Fig. 6). This correlation can be understood by comparison with the results of experiments FT 1 and FT 2. The lithosphere is warmer, and hence weaker, on fast-spreading ridges than on slow-spreading ones. The experiments show that weakening of the lithosphere leads to a widening of the deformed zone. This widening is consecutive to a change in the deformation pattern. A transform zone situated in a 'strong' lithosphere, such as in the MAR, is mainly deformed by a few faults trending roughly parallel to the spreading direction, and accommodating oblique slip on the boundary and strike slip inside the deformed zone. A 'weak' lithosphere as on the EPR permits a complex faulting pattern in the transform zone where the deformation is partitioned between normal faults largely oblique to the transform trend and the strike-slip fault is more or less parallel to the transform orientation (Hékinian *et al.* 1992). Thus structural differences between TZs of the MAR and of the EPR (Figs 1a and b) are explained by strength differences between slow- and fast-spreading systems.

The Tjörnes fracture zone in North Iceland is approximately 100 km wide and has a lateral offset of 120 km. The deformation area extends both offshore and onshore. Offshore, bathymetric and seismic studies indicate that within the deformed zone there is a series of *en-échelon* half-grabens, which are bounded by faults roughly parallel to the ridge axis, i.e. north–south (MacMaster *et al.* 1977; Gudmundsson *et al.* 1993; Rögnvaldsson *et al.* 1998). Onshore, these faults control fjord locations (Fig. 1c). Earthquake alignments offshore suggest the existence of an additional array of N110°–120° strike-slip faults (Einarsson 1991; Rögnvaldsson *et al.* 1998). Inactive strike-slip faults have been reported onshore, prolonging these earthquake alignments (Bergerat *et al.* 1990, 1992). Some of these faults also accommodate significant vertical throw up to 1000 m.

The experiment FT 3 with a large viscous zone above the strike-slip discontinuity shows that these complex fault patterns can be explained by the low strength of the lithosphere in the Tjörnes Fracture Zone, which is an extremely weak transform boundary because it is located above a hotspot. The hotspot increases the regional heat flow and decreases the strength of the lithosphere. The deformed zone is therefore abnormally wide and deformation can be partitioned between two fault sets: (1) a series of strike-slip faults with azimuth close to the spreading direction and (2) a series of normal faults with azimuth highly oblique to the spreading direction. Angles between normal faults and the spreading direction are larger in the Tjörnes Fracture Zone than in experiment FT 3, probably because the relative strength of the lithosphere in Iceland is even lower than in the model and because the spreading direction is not strictly parallel to the transform trend. Fig. 7 compares the strength differences between an oceanic rift and a hotspot in cases of slow and fast-spreading contexts. The strength was estimated from the thickness of the upper brittle layer, which provides good criteria—easy to estimate and sufficient for the this problem. Fig. 7 illustrates that for a given spreading rate the size of the hotspot and the distance controls the strength: it reaches a small value close to the hotspot or close to the ridge axis. Furthermore, increasing the

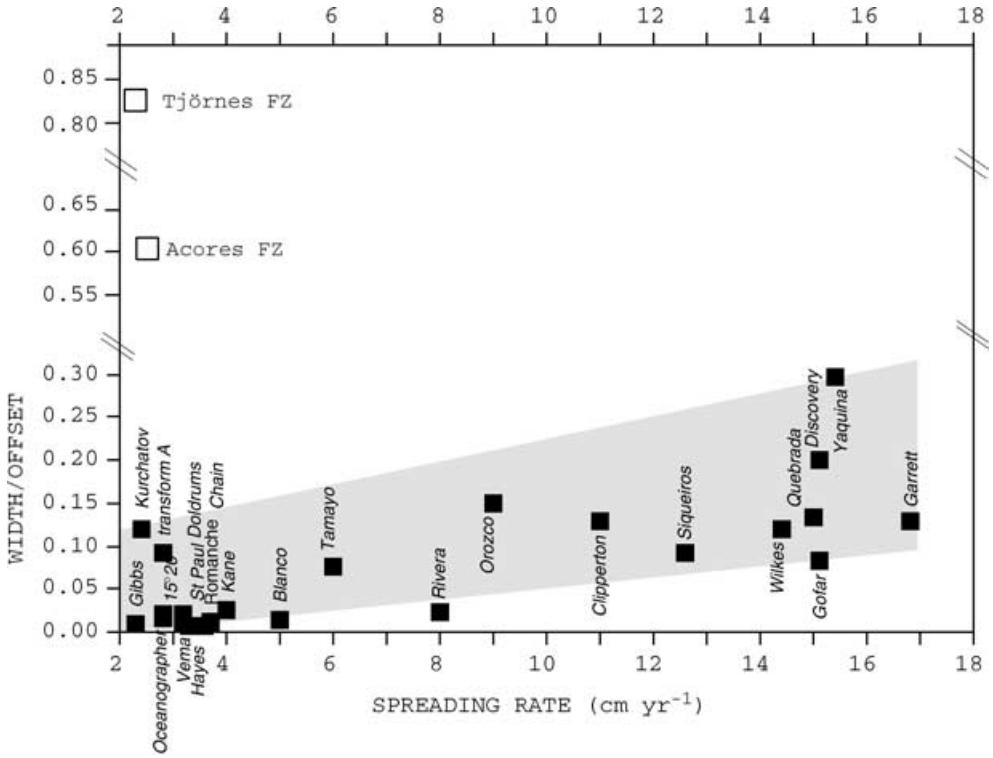

Figure 6. Spreading rate plotted against width/offset for 24 oceanic transform zones on both slow- and fast-spreading ridges (the names are written in italic). The width, measured at the centre of the transform zone, is normalized to the offset in order to reduce the effect of this parameter on the width, as demonstrated by Mauduit & Dauteuil (1996). The data display a good fit between the spreading rate and normalized width, except in the presence of a hotspot.

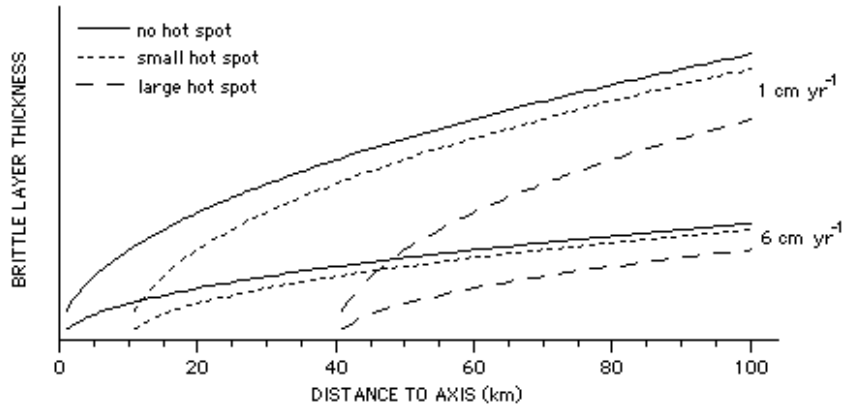

Figure 7. Estimated relative strength of the oceanic lithosphere in different contexts: slow- and fast-spreading rates in the absence and in the presence of a small and a large hotspot. The strength is evaluated from the thickness of the upper brittle layer, which provides a sufficient estimate for our calculation. The value of the spreading rate corresponds to the half rate.

spreading rate decreases the strength. This transform zone trends at N115°–120° (Fig. 1) while the spreading occurs at N104°, showing that the Tjörnes TZ is subjected to a transtensive deformation. Based on different methods, Foulger *et al.* (1992), Hofton & Foulger (1996) and Angelier *et al.* (2000) have reported an abnormal extensive component, roughly perpendicular to the TZ orientation that can be attributed to the slight obliquity.

5 CONCLUSION

Transform zones display different structural patterns commonly assumed to be controlled by the transform offset. Our model results reveal that the lithosphere strength and the flowing of the deep viscous layer can also modify fault patterns of transform zones: a decrease in lithospheric strength widens the deformed zone and diffuses the deformation. Widening of the transform zone is accompanied by the formation of normal faults oblique to the spreading direction and by changes in partitioning between normal and strike-slip faults. In natural cases, the lithospheric strength is related to the spreading rate (a higher rate decreases the strength), to the regional heat flow (for instance, a hotspot drastically decreases the strength) and to the TZ length (a small offset juxtaposes two hot plates decreasing lithospheric strength). Often the TZ have been seen as a simple narrow frontier between different domains, this study shows that this boundary can be localized or more diffuse depending on the local lithospheric strength.

ACKNOWLEDGMENTS

We gratefully acknowledge the assistance of Jean-Jacques Kermarec for his technical help during the experimentation. August Gudmunsson is thanked for his encouragement. We thank P. Cobbold for his comments. This work was conducted under the European program PRENLAB.

REFERENCES

Acocella, V., Faccenna, C., Funiciello, R. & Rossetti, F., 1999. Sand-box modelling of basement-controlled transfer zones in the extensional domains, *TerraNova,* **11,** 149–156.

Angelier, J., Borgerat, T. & Homberg, C., 2000. Variable coupling across weak oceanic transform faults, T'letyjarskagi, Iceland, *Terra Nova,* **12,** 97–101.

Benes, V. & Davy, P., 1996. Modes of continental lithospheric extension: experimental verification of strain localization processes, *Tectonophysics,* **254,** 69–87.

Bergerat, F., Angelier, J. & Villemin, T., 1990. Fault systems and stress patterns on emerged oceanic ridges: a case study in Iceland, *Tectonophysics,* **179,** 183–197.

Bergerat, F., Angelier, J. & Villemin, T., 1992. Système de failles et états de contraintes sur une dorsale émergée: l'Islande, *C.R. Acad. Sci. Paris,* **307,** 1397–1403.

Bergman, E.A. & Solomon, S.C., 1992. On the strengh of oceanic fracture zones and their influence on intraplate stress field, *J. geophys. Res.,* **97,** 15 395–15 377.

Bourgeois, O., 1998. Processus d'extension lithosphèrique en Islande. Interactions avec les calottes glaciaires quaternaires, University thesis, Rennes, *Mém. Géosci. Rennes,* **96,** 280.

Buck, W.R., 1991. Modes of continental lithospheric extension, *J. geophys. Res.,* **96,** 20 161–20 178.

Chen, Y., 1989. A mechanical model for the inside corner uplift at a ridge-transform intersection, *J. geophys. Res.,* **94,** 9275–9282.

Chen, Y.J. & Phipps Morgan, J., 1996. The effect of spreading rate, the magma budget, and the geometry of magma emplacement on the axial heat flux at mid-ocean ridge, *J. geophys. Res.,* **101,** 11 475–11 482.

Choukroune, P., Francheteau, J. & Hekinian, R., 1984. tectonics of the East Pacific Rise near 12°50′N: a submersible study, *Earth planet. Sci. Lett.,* **68,** 115–127.

Dauteuil, O. & Brun, J.-P., 1993. Oblique rifting in a slow-spreading ridge, *Nature,* **361,** 145–148.

Dauteuil, O. & Mart, Y., 1998. Faulting pattern, ductile deformation, and vertical motion in strike-slip provinces: anolog modeling, *Tectonics,* **17,** 303–310.

Davy, P. & Cobbold, P.R., 1991. Experiments of a 4-layer continental lithosphere, *Tectonophysics,* **188,** 1–25.

Davy, P., Hansen, A., Bonnet, E. & Shou-Zhu Zhang, 1995. Localization and fault growth in layered brittle–ductile systems: implications for deformations of the continental lithosphere, *J. geophys. Res.,* **100,** 6281–6294.

Einarsson, P., 1991. Earthquakes and present-day tectonism in Iceland, *Tectonophysics,* **189,** 261–279.

Foulger, G.R., Jahn, C.-H., Seeber, G., Einarsson, P., Julian, B.R. & Heki, K., 1992. Post-rifting stress relaxation at divergent plate boundary in Northeast Iceland, *Nature,* **358,** 488–490.

Grindlay, N.R. & Fox, P.J., 1993. Lithospheric stresses associated with non-transform offsets of the Mid-Atlantic Ridge: implications from a finite element analysis, *Tectonics,* **12, 4,** 982–1003.

Gudmundsson, A., Brynjolfsson, S. & Jonsson, M.T., 1993. Structural analysis of a transform fault-rift zone junction in North Iceland, *Tectonophysics,* **220,** 205–221.

Hékinian, R., Bideau, D., Cannat, M., Francheteau, J. & Hébert, R., 1992. Volcanic activity and crust–mantle exposure in the ultrafast Garrett Transform Fault near 13°28′S in the Pacific, *Earth planet. Sci. Lett.,* **108,** 259–275.

Hofton, M.A. & Foulger, G.R., 1996. Postrifting anelastic deformation around the spreading plate boundary, north Iceland, 1. Modeling of the 1987–1992 deformation field using a viscoelastic Earth structure, *J. geophys. Res.,* **101,** 25 403–25 421.

Kohlstedt, D.L., Evans, B. & Mackwell, S.J., 1995. Strength of the lithosphere: contraints imposed by laboratory experiments, *J. geophys. Res.,* **100,** 17 587–17 602.

Lagabrielle, Y., Garel, E., Dauteuil, O. & Cormier, M.-H., 2001. Extensional faulting and caldera collapse in the axial region of fast spreading ridges: analog modelling, *J. geophys. Res.,* **106,** 2005–2015.

Lin, J. & Parmentier, E.M., 1989. Mechanism of lithospheric extension at mid-ocean ridges, *Geophys. J.,* **96,** 1–22.

Lin, J. & Parmentier, E.M., 1990. A finite amplitude necking model of rifting in brittle lithosphere, *J. geophys. Res.,* **95,** 4909–4923.

Macdonald, K.C., 1982. Mid-ocean ridges: fine scale tectonic, volcanic and hydrothermal processes within the plate boundary zone, *Ann. Rev. Earth Planetary Sci.,* **10,** 155–190.

MacMaster, R.L., Schilling, J.G. & Pinet, P.R., 1977. Plate boundary within Tjörnes Fracture Zone on Northern Iceland's insular margin, *Nature,* **269,** 663–668.

Mauduit, T. & Dauteuil, O., 1996. Small-scale models of oceanic transform zones, *J. geophys. Res.,* **101,** 20 195–20 209.

Phipps Morgan, J. & Forsyth, D.W., 1988. Three-dimensional flow and temperature perturbations due to a transform offset: effects on oceanic crustal and upper-mantle structure, *J. geophys. Res.,* **93,** 2955–2966.

Phipps Morgan, J. & Parmentier, E.M., 1984. Lithospheric stress near a ridge-transform intersection, *Geophys. Res. Lett.,* **11,** 113–116.

Riedel, W., 1929. Zur Mechanic Geologischer Brucherscheinungen, *Z. Min. Geol. Pal.,* **1929B,** 354–368.

Rögnvaldsson, S.T., Gudmundsson, A. & Slunga, R., 1998. Seismotectonic analysis of the Tjörnes Fracture zone, an active transform fault in north Iceland, *J. geophys. Res.,* **103,** 30 117–30 129.

Shaw, W.J. & Lin, J., 1996. Models of ocean ridge lithospheric deformation: dependence on crustal thickness, spreading rate and segmentation, *J. geophys. Res.,* **101,** 17 977–17 993.

Stoddard, P.R., 1992. On the relations between transform zones resistance and plate motion, *J. geophys. Res.,* **97,** 17 637–17 650.

Thibaud, R., Dauteuil, O. & Gente, P., 1999. Faulting pattern along a slow-spreading ridge segment: a consequence of along axis variation in lithospheric rheology, *Tectonophysics,* **312,** 157–174.

Tron, V. & Brun, J.-P., 1991. Experiments on oblique rifting in brittle–ductile systems, *Tectonophysics,* **188,** 71–84.

Tuckwell, G.W., Bull, J.M. & Sanderson, D.J., 1999. Mechanical control of oceanic plate boundary geometry, *Tectonophysics,* **313,** 265–270.

Watts, A.B., Bodine, J.H. & Steckler, M.S., 1980. Observation of flexure and the state of stress in the oceanic lithosphere, *J. geophys. Res.,* **85,** 6369–6376.

Weijermars, R., 1986a. Finite strain of laminar flow can be visualized in SGM 36-polymer, *Naturwisseschaften,* **73,** 33.

Weijermars, R., 1986b. Flow behaviour and physical chemistry of bouncing putties and related polymers in view of tectonic laboratory application, *Tectonophysics,* **124,** 325–358.